

Article

W-Doped ZnO Photocatalyst for the Degradation of Glyphosate in Aqueous Solution

Mariaconcetta Russo, Giuseppina Iervolino * and Vincenzo Vaiano 

Department of Industrial Engineering, University of Salerno, Via Giovanni Paolo II, 132, 84084 Fisciano, SA, Italy; marrusso@unisa.it (M.R.); vvaiano@unisa.it (V.V.)

* Correspondence: giervolino@unisa.it; Tel.: +39-089-964006; Fax: +39-089-9694057

Abstract: In this paper, the photocatalytic degradation of glyphosate by zinc oxide (ZnO) photocatalysts doped with tungsten (W) was investigated under solar simulated light. The photocatalysts were successfully synthesized through a simple precipitation method and subsequently characterized by different techniques: Raman spectroscopy, UV-Vis, N₂ adsorption at −196 °C, X-ray diffraction, and SEM analysis. In particular, all the prepared catalysts were characterized by a crystallite size of about 28 nm and a hexagonal wurtzite structure. After the W doping, the bandgap energy decreased from 3.22 of pure ZnO to 3.19 for doped ZnO. This allowed us to obtain good results in terms of glyphosate degradation and simultaneous mineralization under solar simulated lamps, making the process environmentally friendly and with almost zero energy costs. In particular, the best photocatalytic performance was obtained with 100 W-ZnO (prepared with 1.5 mol% of W). With this catalyst, after 180 min of exposure to solar simulated light, the glyphosate degradation and mineralization was equal to 74% and 30%, respectively. Furthermore, it has been shown that the best catalyst dosage was equal to 1.5 g/L. The study on the influence of pH evidenced that the best photocatalytic performances are obtained at spontaneous (neutral) pH conditions. Finally, to determine the main reactive species in the glyphosate oxidation, the effects of different radical scavengers were tested. The results evidenced that the glyphosate oxidation mechanism seems to be related mainly to the O₂^{•−} generated under simulated solar light irradiation, but also in minor part to h⁺.

Keywords: glyphosate; photocatalysis; solar light; W-doped ZnO



Citation: Russo, M.; Iervolino, G.; Vaiano, V. W-Doped ZnO Photocatalyst for the Degradation of Glyphosate in Aqueous Solution. *Catalysts* **2021**, *11*, 234. <https://doi.org/10.3390/catal11020234>

Received: 22 January 2021

Accepted: 7 February 2021

Published: 9 February 2021

Publisher's Note: MDPI stays neutral with regard to jurisdictional claims in published maps and institutional affiliations.



Copyright: © 2021 by the authors. Licensee MDPI, Basel, Switzerland. This article is an open access article distributed under the terms and conditions of the Creative Commons Attribution (CC BY) license (<https://creativecommons.org/licenses/by/4.0/>).

1. Introduction

The protection of water from pollution is just one of the aspects involving the most important problem of our existence, which is the protection and conservation of the environment in which we live. In fact, there is an urgent need to prevent contamination of available water resources from various kinds of pollutants such as pesticides particularly used in agriculture. In fact, the indiscriminate use of pesticides to increase agricultural production has led to the contamination of water, generating serious environmental damage [1]. Pesticides are chemical contaminants used to kill different types of pests that cause damage to cultures. Due to their nature, these compounds are potentially toxic to other organisms, including humans [2]. Effluents from chemical and agrochemical industries contain several organic compounds such as solvents and pesticides [3]. Recently, a highly controversial herbicides that has attracted public attention is glyphosate, which is one of the most used herbicides worldwide and is defined as a carcinogenic substance by IARC. The intense use of this herbicide had an impact on key functions of the rhizosphere. The effects include reduced absorption of essential micronutrients by plants, greater vulnerability to diseases, and reduction of nitrogen fixation, with a paradoxical yield of lower crops and changes in bacterial composition [4]. Glyphosate is a systemic herbicide, post-emergent, non-selective and belonging to the chemical group of phosphonate amino acids. It acts as a potent inhibitor of the activity of the enzyme 5-enolpyruvylshikimate

3-phosphate synthase (EPSPS), which is a key enzyme of the shikimate pathway, responsible for aromatic amino acid synthesis reactions in algae, plants and fungi [5]. A lot of studies showed that glyphosate could be degraded by microorganisms and plants to yield aminomethylphosphonic acid (AMPA) and sarcosine, which could be further degraded into the water, carbon dioxide, and phosphate, although the slower degradation of AMPA had been reported in some instances [6]. The presence of glyphosate in the aquatic environment causes serious environmental risks. Traditional degradation methods, such as biological and physicochemical ones, have been applied for the removal of glyphosate. However, processes such as filtration using sand, ultrafiltration, reverse osmosis, adsorption by activated charcoal and biological degradation are expensive and require large infrastructure investments and some are specific to particular contaminants [7,8]. If the operating conditions are not controlled, biological processes can generate by-products, such as metabolites, characterized by potentially higher toxicity [9]. Advanced oxidation processes (AOPs) are considered among the most promising processes for wastewater treatments containing pesticides. The advantages of these processes are related to the high percentage of degradation of organic pollutants [10–13] but also to the ability to produce hydrogen, promote CO₂ reduction, NO_x reduction or ammonia synthesis, and to be environmentally friendly processes characterized by low energy consumption [14–17]. Many studies on the photocatalytic degradation of glyphosate have been published, many of which used TiO₂ based photocatalysts [18–26]. However, recently, a semiconductor that has attracted scientific attention for water treatment applications is zinc oxide (ZnO), due to it is relatively cheaper compared to TiO₂. It can be considered as a promising semiconductor with higher photocatalytic efficiency in the degradation of several organic contaminants in presence of different pH conditions [27–31]. In fact, its use has been widely reported in the literature in the degradation of various kinds of aqueous contaminants, such as pharmaceutical compounds [31], dyes [32] or metals such as arsenic [33]. Furthermore, it was also applied in fixed or floating bed reactors, in which ZnO had been deposited on macroscopic supports such as glass spheres [32] or polystyrene pellets. These data allow to define ZnO as a catalyst useful for the degradation of different types of contaminants, both present in industrial wastewater (such as dyes) and present in urban wastewater (for example emerging contaminants, therefore pharmaceutical compounds), and also in case of water treatment intended for potable use for the removal of metals. However, ZnO is characterized by a wide bandgap (3.27 eV) and it limits its photoactivity only under UV light. This means that only a small percentage (about 5%) of the sunlight that reaches the earth's surface can be used to activate this photocatalyst [34,35]. Considering the recent studies about the photocatalytic degradation of glyphosate, most of them are based on the use of UV light. Unfortunately, it must be considered that although UV light guarantees the activation of a large group of semiconductors, adequate equipment is required for its use [36]. Therefore, given this last observation and considering that nowadays the demand for processes based on the use of low-cost energy resources is increasing, it is interesting to focus attention on the synthesis of photocatalysts activated by visible (solar) light [37]. Moreover, as regards the ZnO, it should also be noted that this semiconductor is characterized by a recombination of the hole-electron pair, which disadvantages its photocatalytic activity. To reduce this recombination and to decrease the bandgap energy, ZnO can be doped with selected elements, such as Eu, Ce, and Cu [25,38–40]. Recently, tungsten oxides have attracted much interest due to their unique physical and chemical properties among various oxide semiconductors [41–43]. Tungsten oxides have a variety of nonstoichiometric phases (expressed as WO_x (2 ≤ x < 3)), such as WO_{2.9}, W₁₈O₄₉ (WO_{2.72}), and WO₂, which possess unique oxygen vacancies and crystal shear planes [44]. ZnO photocatalyst coupled with WO₃ is used for photooxidative degradation of organic pollutants. For example, it is reported the synthesis of nanosized MO_x-ZnO (M=W, V, Fe) composite powders by spray pyrolysis and their visible-light-driven photocatalysis in gas-phase acetaldehyde decomposition [45]. Another study discusses the use of W-doped ZnO nanocomposite for the photodegradation of methylene blue in aqueous solution under UV and visible light

irradiation [46]. Additionally, an improvement of photocatalytic activity of WO_3 loaded Ag-ZnO for acid black-1 degradation by UV-A light is also observed [47]. With regard to the photocatalytic degradation of glyphosate, a recent paper reports the photocatalytic performances of ZnO nanoparticles under UV irradiation [48], whereas no specific study devoted to the use of the W-doped ZnO photocatalyst in the removal of glyphosate is present in the literature. For this reason, this work aims to study the photocatalytic degradation of glyphosate from aqueous solutions using W-doped ZnO, in presence of visible light and also under solar simulated light. The effect of different parameters (W amount, different light sources, catalyst dosage, glyphosate initial concentration and initial pH of solution) on the photocatalytic activity in terms of glyphosate degradation and mineralization was investigated. Finally, the main reactive oxygen species (ROS) responsible for glyphosate degradation were identified.

2. Results and Discussion

2.1. Catalyst Characterization

2.1.1. Raman Analysis

Raman results are reported in Figure 1 showing the spectra ranging from 200 to 700 cm^{-1} for doped catalysts in comparison with undoped ZnO. The results evidence the presence of characteristics bands at 333, 381, 436, and 581 cm^{-1} relative to ZnO [49]. The strong and sharp band visible at 436 cm^{-1} is equivalent to non-polar optical phonon E2 (high) of wurtzite ZnO while the band at 333 cm^{-1} is assigned to the second-order Raman spectrum arising from zone boundary phonons of the hexagonal ZnO [50]. The signal at 391 cm^{-1} is attributed to A1(TO) mode while the peak at 581 cm^{-1} corresponds to E1 (LO) mode [49]. No significant difference in the bands position is observed between the Raman spectrum of pure ZnO and W-ZnO samples. However, the doping with tungsten causes a decrease in the intensity of the peaks—as the tungsten load increases, the intensity of the peaks decreases. This behavior is consistent with literature data dealing with ZnO doped with different metals [51,52]. In detail, the decrease of Raman bands may be explained with the insertion of W into the ZnO lattice, which induces the change of the local environment around the host, altering the normal lattice symmetry [53] and without changing the hexagonal structure of ZnO. Additionally, no additional Raman bands appear in the spectra of the doped samples, confirming good incorporation of W into the ZnO lattice.

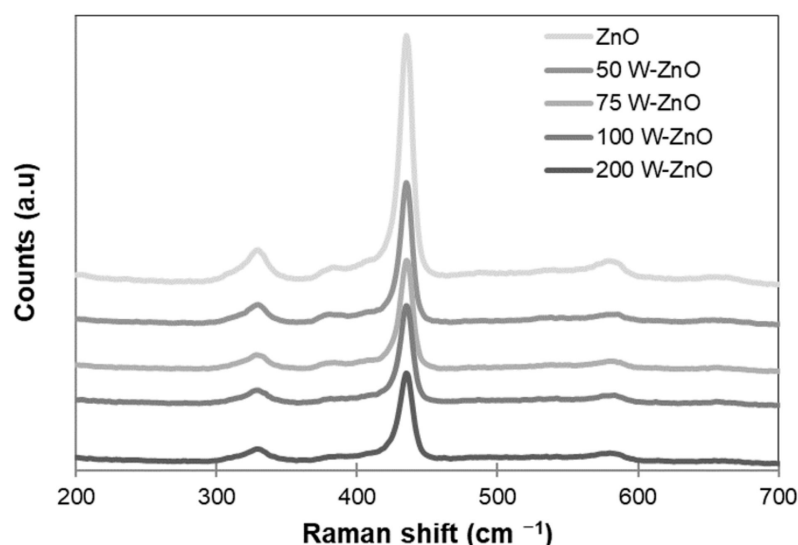


Figure 1. Raman measurements of undoped ZnO and W-doped ZnO photocatalysts in the range $200\text{--}700\text{ cm}^{-1}$.

2.1.2. BET Surface Area

The specific surface areas (SSA) of ZnO and W-ZnO samples are reported in Table 1. It is possible to see that the incorporation of dopant ions causes a variation of SSA values. In particular, from the data, it is possible to note an increase in the surface area for the samples doped with tungsten (for 100 W-ZnO the SSA was equal to 13 m²/g) compared to the non-doped ZnO (6 m²/g). The photocatalytic activity is influenced by the specific surface, therefore this trend of the surface area in the doped samples can determine the presence of additional photoactive sites available for the photocatalytic activity [31]. The adsorption and desorption isotherms for undoped ZnO and for 100 W-ZnO are reported in Figure S1 (Supplementary material). As it can be seen from the graphs, the adsorption and desorption isotherms of ZnO and 100 W-ZnO are almost similar: they present the same shape but in the case of the doped sample the volume of N₂ adsorbed is higher than the undoped one. In both cases, the nitrogen adsorption isotherm is a typical II-type curve (IUPAC classification) and they show the characteristic behavior of monolayer-multilayer adsorption on the open surface of closed pores in agreement with the literature [54] (Figure S1).

Table 1. Characteristics of the prepared photocatalysts.

Photocatalyst	W Nominal Amount (mol%)	W Measured Amount (XRF) (mol%)	SSA ¹ (m ² /g)	Band Gap Energy (eV)	Crystallinity Size ² (nm)
ZnO	0	0	6	3.23	39.82
50 W-ZnO	0.7	0.65	12	3.22	-
75 W-ZnO	1.1	1.15	13	3.22	-
100 W-ZnO	1.5	1.6	13	3.21	38.02
200 W-ZnO	2.9	2.85	17	3.19	-

¹ B.E.T. method. ² Scherrer equation

2.1.3. UV-Vis Diffuse Reflectance Spectra (UV-Vis DRS)

The UV-Vis DRS spectra of the prepared photocatalysts are reported in Figure 2. The undoped ZnO spectrum showed an absorption onset at approximately 390 nm, which is in good agreement with the intrinsic energy bandgap of ZnO (3.23 eV) [55]. As reported in the literature, this behavior can be explained as the electronic transition from O2p to Zn3d, linked to the passage from the valence band to the conduction one, which is in agreement to the literature [56]. Doping with tungsten induces for ZnO photocatalyst an enhancement in the light absorption in the UV region (Figure 2a). In addition, the doping showed an improvement of the absorbance properties in the visible region (Figure 2b). The band-gap energy of the photocatalysts (summarized in Table 1) is calculated by the data obtained from UV-vis DRS spectra (Figure 3) for undoped ZnO and 100 W-ZnO). The band-gap energy is reduced from 3.23 eV for undoped ZnO to 3.19 eV for 200 W-ZnO when the W content was increased, as reported in literature [57]. The band gap reduction was due to the electronic transition from the levels of donors formed with the dopant to the conduction band of the host photocatalysts [43].

2.1.4. XRD Analysis

XRD patterns of undoped and 100 W-ZnO samples are reported in Figure 4a. It is possible to observe peaks located at 2θ 31.7°, 34.4°, 36.2°, 47.7°, 56.5°, 62.7°, and 68.4° corresponding to (1 0 0), (0 0 2), (1 0 1), (1 0 2), (1 1 0), (1 0 3), and (1 1 2) planes, respectively, associated to the typical hexagonal wurtzite structure of ZnO [58]. No diffraction peaks from tungsten oxides or other impurities were detected. The decrease in intensity of XRD patterns of the doped sample with respect to the undoped one could be associated to the ZnO lattice distortion phenomena induced by the doping with W⁶⁺ ion thanks to its lower ionic radius (W⁶⁺ = 0.064 nm and Zn²⁺ = 0.074 nm) [46]. This hypothesis is confirmed by XRD analysis in the range 35.5–37° (Figure 4b.) in which the peak at 2θ = 36.2° indexed as (1 0 1) of undoped ZnO shifts towards a higher angle for 100 W-ZnO. This shift is consistent with the literature about the doping of ZnO with metals having an ionic radius lower

than Zn^{2+} [33] This phenomenon can be attributed to the shrinkage of ZnO crystal lattice induced by the substitution of Zn^{2+} ion by the smaller W^{6+} ion, suggesting, therefore, that W^{6+} can be replaced Zn^{2+} into ZnO lattice without modifying the crystal structure of ZnO [46]. Furthermore, the doping with tungsten induces a minor diminution in photocatalysts crystallite size (Table 1). In particular, the average crystallite size varies from 40 nm for undoped ZnO to 38 nm when the W amount is added. Similar behavior was previously observed in the literature [46]. It is argued that, when some W^{6+} ions entered into the crystal lattice of ZnO, the growth of the ZnO crystallites is inhibited [46].

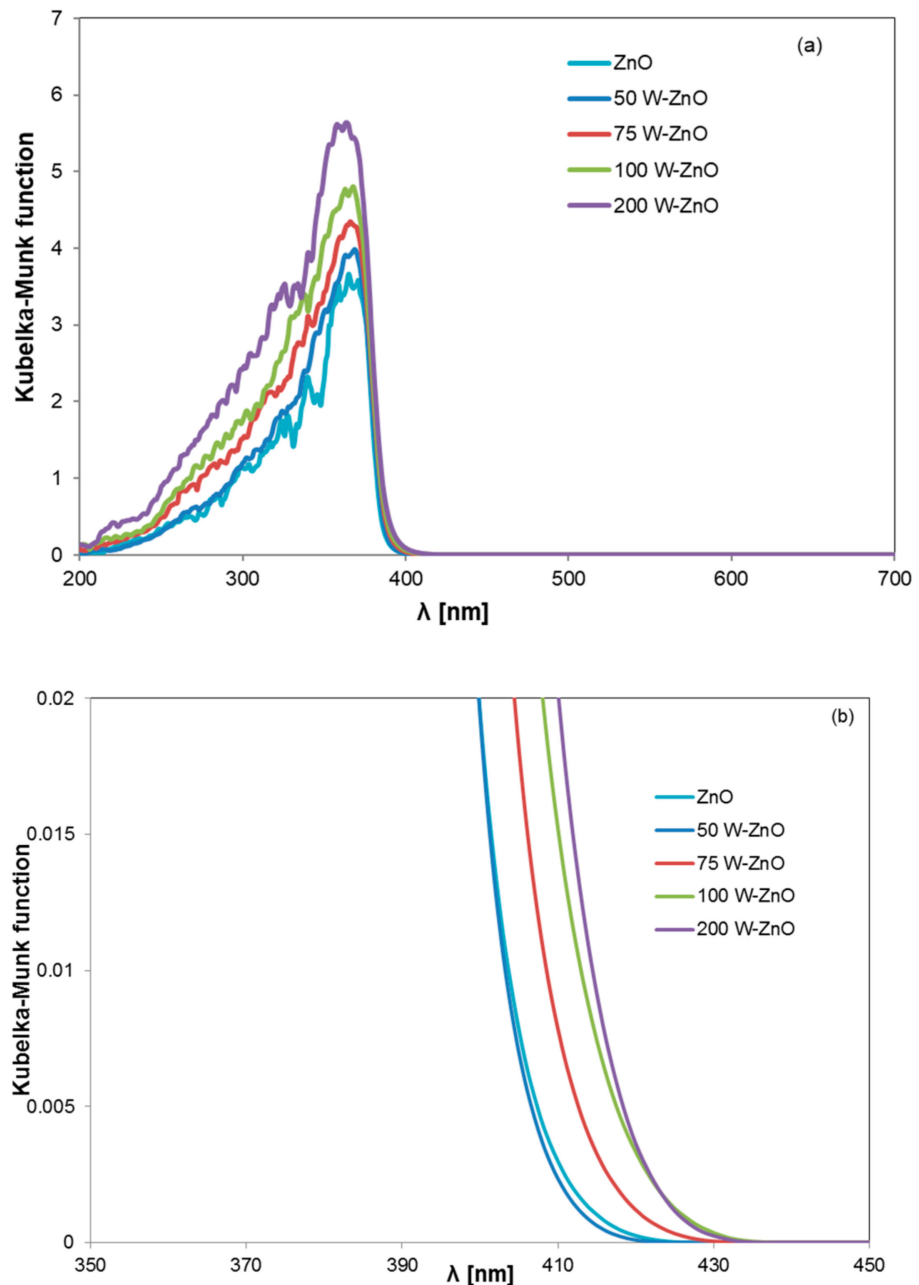


Figure 2. Kubelka-Munk function of ZnO and W-doped ZnO photocatalysts with different W contents in the range 200–700 nm (a) and in the range 350–450 nm (b).

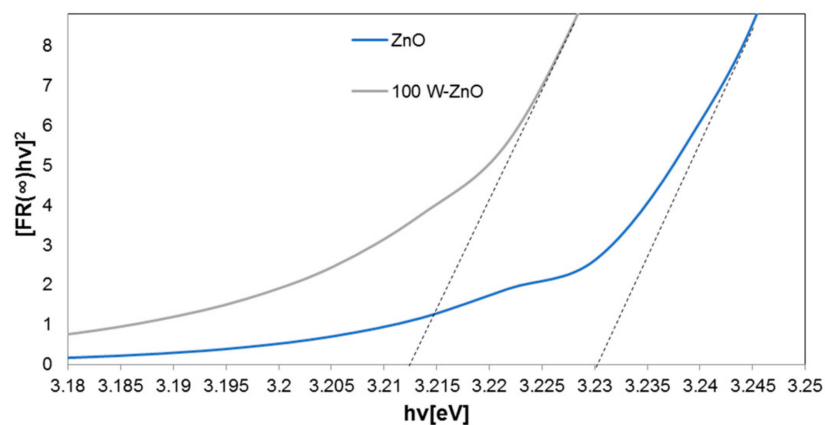


Figure 3. Calculation of band gap for undoped (ZnO) and doped photocatalysts (100 W-ZnO).

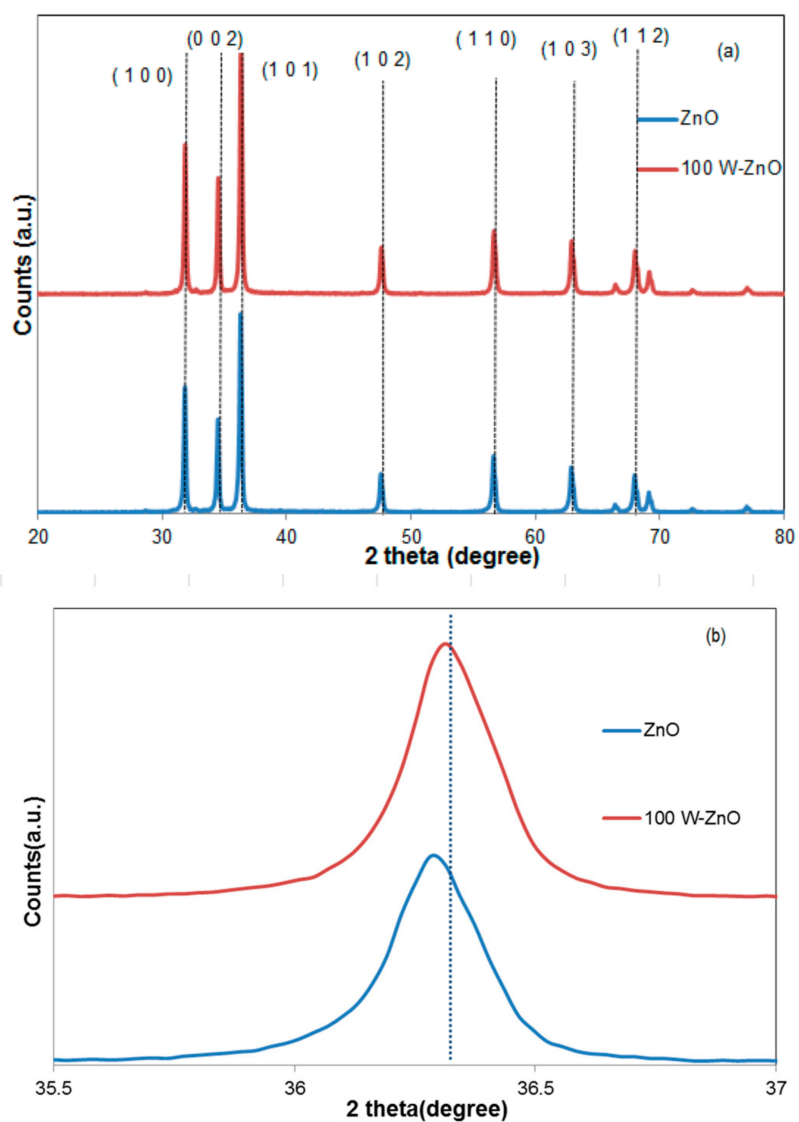


Figure 4. XRD patterns of undoped ZnO and W-doped ZnO photocatalysts in the range 20–80° (a) and in the range 35.5–37° (b).

2.1.5. SEM Analysis

Through SEM microscopy the morphology of the ZnO and W-doped ZnO photocatalysts was investigated. For the sake of brevity, in Figure 5, we only reported the analysis on undoped ZnO and 100 W-ZnO.

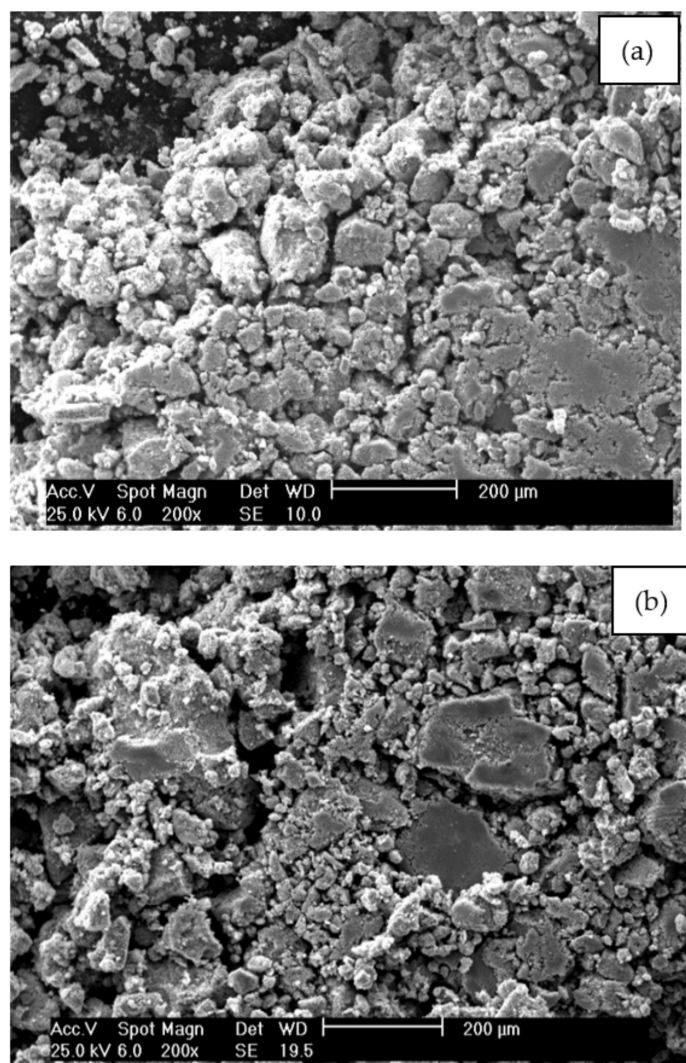


Figure 5. SEM results of ZnO (a) and 100 W-ZnO (b) photocatalysts.

A typical SEM image of ZnO nanoparticles is reported in Figure 5a. In agreement with the literature [46] it is possible to observe that most of the nanoparticles have an irregular shape, more or less spherical, with dimensions less than 100 µm. The 100 W-ZnO sample (Figure 5b) shows a surface morphology similar to bare ZnO (Figure 5a). In addition, in this case it is possible to note a relatively spherical shape for nanoparticles and the presence of nanoparticle agglomerates. These morphology characteristics favor the dispersion of the catalyst in solution, improving the photons absorption.

2.2. Photocatalytic Activity Results

2.2.1. Influence of W Amount

The influence of W amount (from 0.7 to 1.5 mol%) for glyphosate photodegradation was investigated under solar simulated lamps at spontaneous pH and with a photocatalyst dosage equal to 1.5 g/L (Figure 6). During the photolysis test, glyphosate degradation and mineralization were negligible. This result is consistent with the literature [23,59,60] in which it was reported that direct photolysis is usually not an option due to the low efficiency

of most pesticides. As far as the tests in presence of photocatalysts, Figure 6 shows that all the doped samples evidenced higher photocatalytic activity compared with undoped ZnO. As the dopant amount was increased from 0.7 to 1.5 mol%, the degradation and mineralization efficiency increased, but a further increase of the dopant content resulted in a decrease of glyphosate degradation as well as mineralization performances (Figure 7). It is possible to argue that the dopant element acts as a charge trap avoiding the electron-hole recombination rate and improving the interfacial charge transfer to degrade the glyphosate within the optimal molar percentage of dopant (1.5 % mol of W). In agreement with the literature, the increase in W^{6+} ions concentration determines a better e^-/h^+ pairs separation by the large electric field caused by a higher surface barrier and a narrower space charge region [46]. On the other hand, increasing the amount of W^{6+} ions, the depth of light penetration into the ZnO structure significantly exceeds the space charge layer and so the recombination of photogenerated e^-/h^+ pairs becomes easier. Therefore, in order to separate the electron-hole photoinduced pairs, it is necessary to identify the optimal concentration of W^{6+} ions that can correspond to the thickness of the charge layer and to the depth of light necessary for the separation of the charges, as reported in a similar study on the photocatalytic activity of La-ZnO [61]. Furthermore, finding the optimal concentration of W^{6+} ions is necessary to effectively separate the electron-hole pairs, in fact, an excessive amount of W can create a greater number of recombination centers, which worsens the photocatalytic activity.

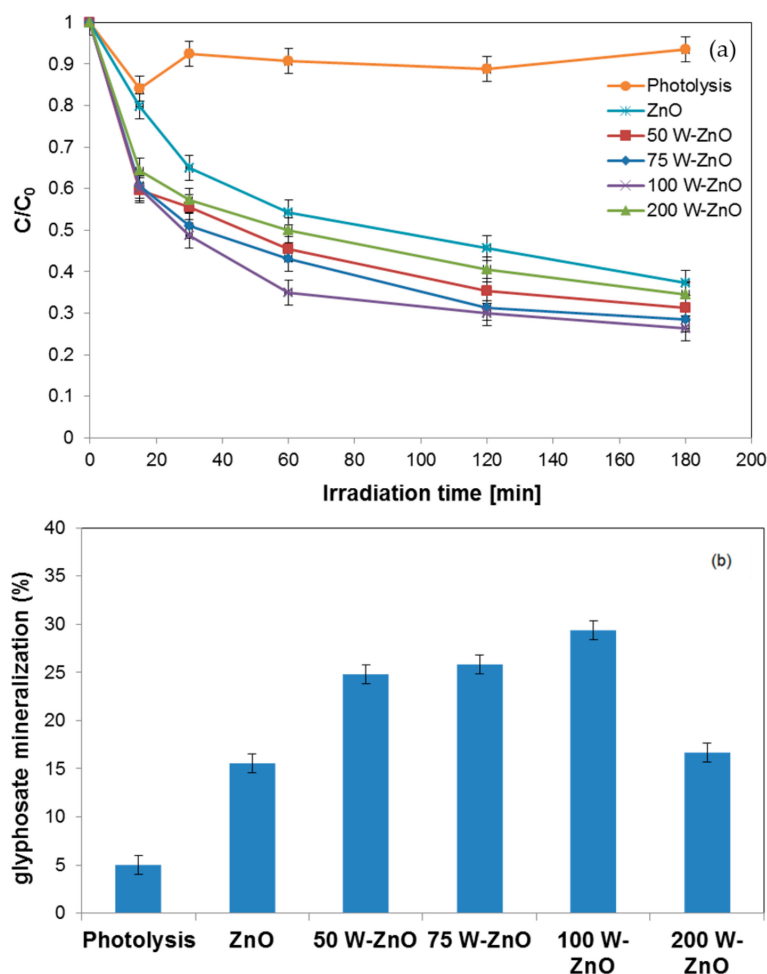


Figure 6. Photocatalytic glyphosate degradation (a) and mineralization (b) at different W nominal amount under the irradiation time; initial glyphosate concentration: 20 mg/L; pH = 7.

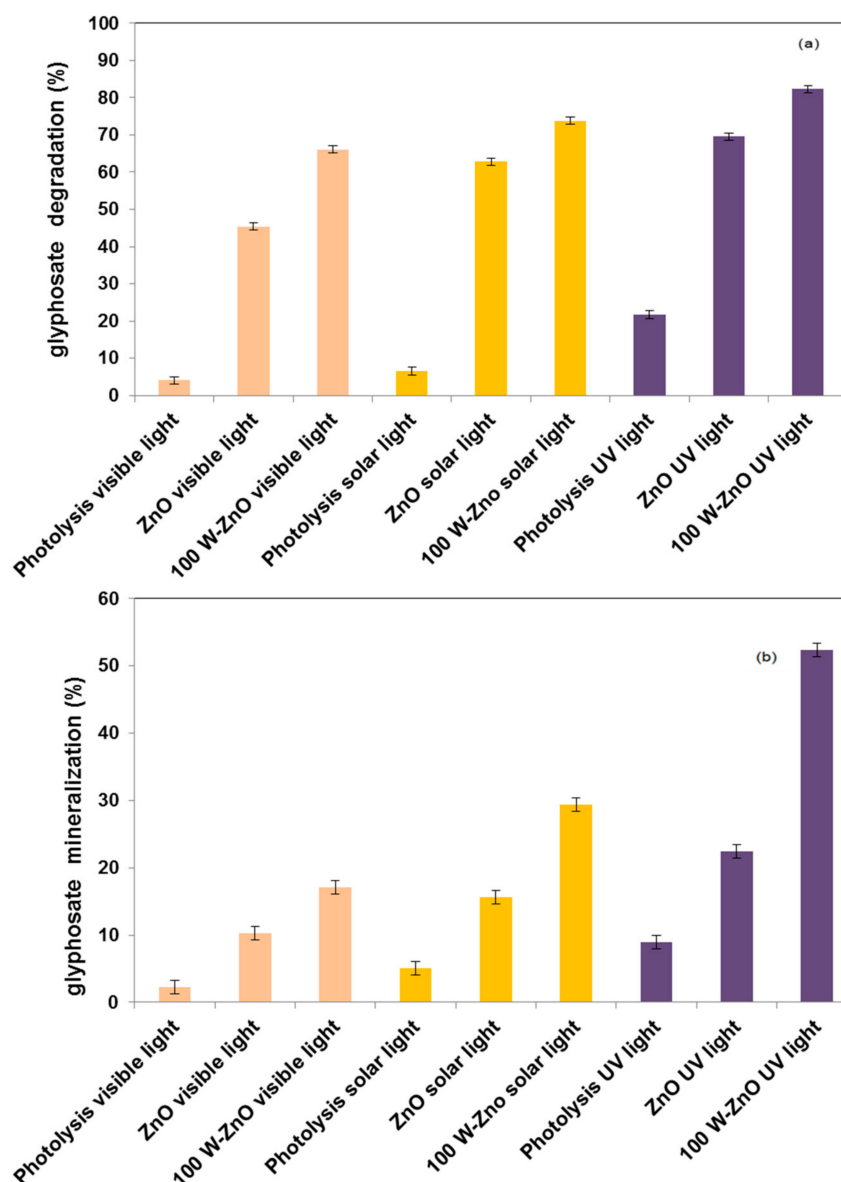


Figure 7. Photocatalytic glyphosate degradation (a) and mineralization (b) of ZnO and 100 W-ZnO under different light sources under the irradiation time; initial glyphosate concentration: 20 mg/L; pH = 7; catalyst dosage = 1.5 g/L.

2.2.2. Influence of Different Light Sources

During the photocatalytic tests, we also analyzed the influence of different light sources with a catalyst dosage of 1.5 g/L and a glyphosate concentration equal to 20 mg/L. Figure 7 compares the values of degradation for pure ZnO and 100 W-ZnO photocatalysts under UV, visible and solar light. The results proved that the best performances were obviously obtained under UV irradiation both in terms of degradation (82%) and mineralization (52%) in 180 min of irradiation. However, interesting results were obtained under solar simulated lamps, reaching a degradation and mineralization efficiency of 74 and 30%, respectively. On the basis of this last result, it was preferred to continue the experimental tests using solar lamps since the possible irradiation with the direct sunlight may be an environmentally friendly process with zero energy costs.

2.2.3. Influence of Catalyst Dosage

Different experimental tests under solar light irradiation were carried out to optimize the photocatalyst dosage. In particular, starting from a glyphosate concentration equal to 20 mg/L, 100 W-ZnO photocatalyst dosages were tested in the range 0.375–3 g/L. Figure 8a,b show glyphosate degradation and mineralization, respectively, after 3 h of solar simulated irradiation time for the different photocatalyst dosages. The graph showed that the photocatalytic efficiency expressed as glyphosate degradation increased up to 1.5 g/L of photocatalyst dosage. With a further increase in the catalyst dosage, the photocatalytic activity worsened, most likely due to the increase in turbidity of the solution which prevented a good photonic distribution on the photocatalytic particles [62].

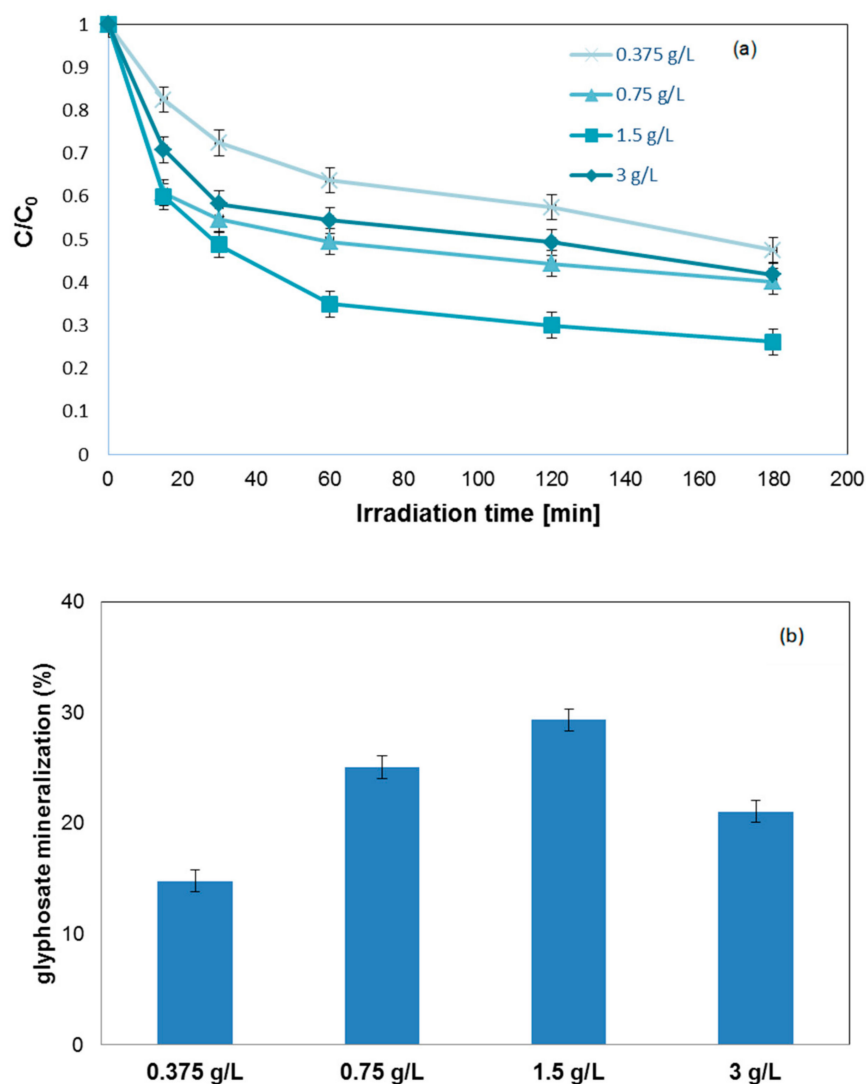


Figure 8. Photocatalytic glyphosate degradation (a) and mineralization (b) at different catalyst dosage for 100 W-ZnO during the irradiation time; initial glyphosate concentration: 20 mg/L; PH = 7.

2.2.4. Influence of pH

Before verifying the influence of pH on the glyphosate degradation, experimental tests regarding the influence of the glyphosate initial concentration were performed (see the Supplementary Material). Specifically, in Figure S2 it is possible to observe that for glyphosate degradation (Figure S2a), similar results were obtained both at 10 mg/L and 20 mg/L of glyphosate initial concentration, while a worsening both in terms of degradation and mineralization (Figure S2b) was found in the case of an initial glyphosate

concentration equal to 40 mg/L. As regards the mineralization (Figure S1b), it can be found that the best result (76% of mineralization) is obtained starting with a solution containing 10 mg/L of glyphosate. On the basis of these results, the influence of pH on the photocatalytic glyphosate degradation was evaluated at an initial glyphosate concentration equal to 10 mg/L.

The effect of pH on the photocatalytic degradation of glyphosate is investigated by varying the pH of the medium from 4 to 10 and keeping constants of the other operating conditions. The results are presented in Figure 9.

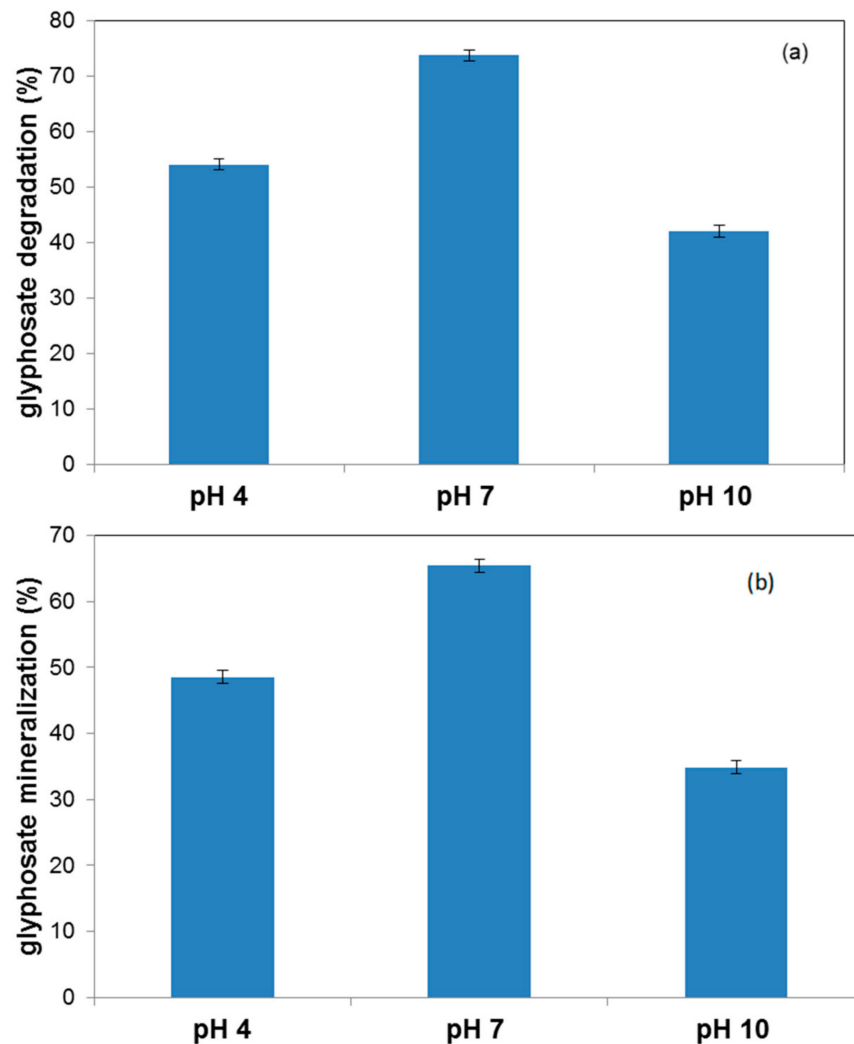
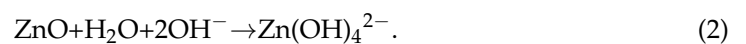


Figure 9. Photocatalytic glyphosate degradation (a) and mineralization (b) at different pH solutions during the irradiation time; glyphosate concentration = 10 mg/L; catalyst dosage = 1.5 g/L.

It is evident that the best photocatalytic performances were achieved at pH = 7. According to the literature [63], ZnO powder tend to dissolve with decreasing the pH (Equation (1)):



In a strongly alkaline environment, ZnO can undergo dissolution according to Equation (2)



The possible formation of photocatalytically inert Zn(OH)_2 surface layers is also to be considered in aqueous media, as shown in Equation (3) [64]:



Therefore, the reduction of photocatalytic activity of ZnO at low and high pH values can originate from:

- acidic/photochemical corrosion of the catalyst;
- alkaline dissolution (Equation (2)) and/or surface passivation with Zn(OH)_2 (Equation (2)) [63]. Furthermore, Equation (2) can interfere with the formation of hydroxyl radicals by decreasing the availability of holes for water or surface OH^- oxidation.

2.2.5. Influence of Scavengers

The mechanism of the catalytic degradation of glyphosate was investigated using different scavenger molecules to identify the main reactive species involved in the photocatalytic process. In particular, *i*-PrOH (10 mM) EDTA (0.2 mM) and benzoquinone (1 mM) have been employed to quench, respectively, (OH^\bullet , h^+ , $\text{O}_2^{\bullet-}$). Figure 10 shows that when isopropanol (IPA) was added, the glyphosate degradation was not influenced and this demonstrated that hydroxyl radicals (OH^\bullet) were not the main reactive species, unlike EDTA, which determines a negative effect on the photodegradation. This behavior suggests the important role of h^+ but a very interesting result is obtained when benzoquinone was added (superoxide scavenger): the photocatalytic activity was suppressed significantly under these conditions. This result allows to define that the main role in the photocatalytic degradation process of glyphosate is played by superoxide. From the tests, h^+ and superoxide prove to be the two main active species of the W-ZnO photocatalyst in the degradation of glyphosate in the presence of simulated irradiation and in particular superoxide plays a more significant role. Comparable results were obtained in another study based on the use of $\text{BiOBr/Fe}_3\text{O}_4$ nanocomposites under visible light irradiation for glyphosate degradation [37].

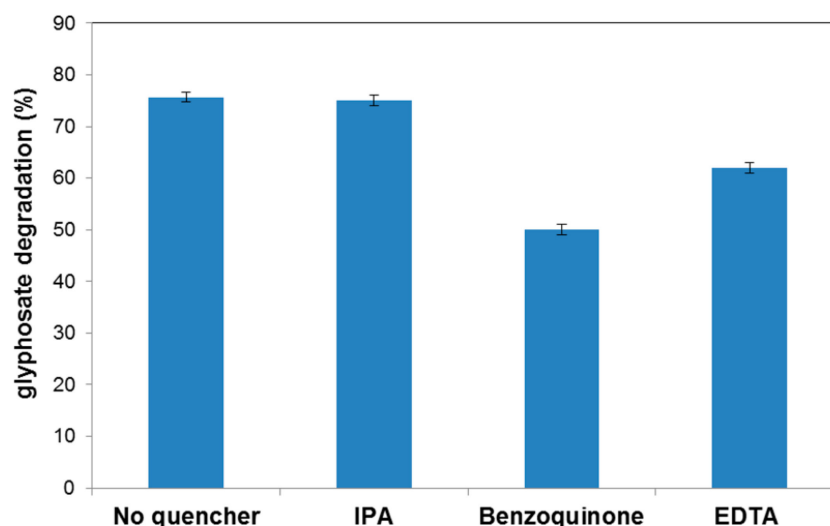


Figure 10. Trapping experiment of active species during the photocatalytic degradation of glyphosate under solar irradiation; initial glyphosate concentration: 10 mg/L; pH = 7; catalyst dosage = 1.5 g/L.

3. Material and Methods

3.1. Materials

Zinc acetate ($\text{ZnC}_4\text{H}_6\text{O}_4$), ammonium metatungstate hydrate ($\text{H}_{26}\text{N}_6\text{O}_{40}\text{W}_{12}$), sodium hydroxide (NaOH), the herbicide glyphosate ($\text{C}_3\text{H}_8\text{NO}_5\text{P}$), ninhydrin ($\text{C}_9\text{H}_6\text{O}_4$) and sodium molybdate (Na_2MoO_4) were supplied by Sigma-Aldrich.

3.2. Photocatalysts Preparation

3.2.1. Undoped ZnO

Undoped ZnO photocatalyst was synthesized through precipitation method. As the first step, 5 g of zinc acetate is dissolved in 75 mL of distilled water. The suspension was maintained in agitation until the complete solubilization of the zinc acetate in distilled water. The precipitation was induced by adding a solution of NaOH 2 M (2 g NaOH/25 mL H_2O). Once the suspension was well mixed, it was transferred to 50 mL Falcon Isolab to be centrifuged. As follows, the precipitate was washed with distilled water and then calcined for 2 h at 600 °C in a muffle furnace.

3.2.2. W-doped ZnO

Ammonium metatungstate hydrate $\text{H}_{26}\text{N}_6\text{O}_{40}\text{W}_{12}$ was added to the solution during the doping procedure. Specific amounts of it were completely dissolved into the zinc acetate solution inducing subsequently the precipitation by sodium hydroxide addition. The final product was separated from the stock solution by centrifugation, then dried and subsequently subjected to a calcination temperature of 600 °C for 2 h. The W nominal, reported as a molar percentage, was calculated through Equation (4):

$$\% \text{ mol W} = \frac{n \text{ W}}{n \text{ W} + n \text{ Zn}} \times 100, \quad (4)$$

where:

$n \text{ W}$ is the number of moles of W used in the synthesis calculated as:

$n \text{ H}_{26}\text{N}_6\text{O}_{40}\text{W}_{12} \times 12$;

$n \text{ Zn}$ is the number of moles of $\text{Zn}(\text{CH}_3\text{COO})_2 \cdot 2\text{H}_2\text{O}$ used during the preparation;

The list of all photocatalysts synthesized is reported in Table 1.

3.3. Photocatalysts Characterization

Different techniques were used for the catalysts characterization. In particular, the specific surface area (SSA) was performed by Brunauer-Emmett-Teller (BET) method using N_2 physical adsorption at -196 °C (Costech Sorptometer 1042) after a pretreatment at 150 °C for 1 h in He flow (99.9990%). The Raman spectra of the prepared photocatalyst have been processed with a Dispersive MicroRaman system (Invia, Renishaw), equipped with a 514 nm laser, varying from 100 to 2000 cm^{-1} Raman shift. The crystal phases of the photocatalyst were determined by XRD analysis (Bruker D8 diffractometer Bruker Corporation, Madison, WI, USA), in the range 20–80 degrees, and 30–34 degree. With Scherrer's equation, the average crystallite size was calculated. The W total amount was realized by the X-ray fluorescence spectrometry (XRF) in a thermoFischer ARL QUANT'X EDXRF spectrometer using a rhodium standard tube as the origin of radiation and with Si-Li drifted crystal sensor. The UV-vis reflectance spectra of the catalysts were observed by a Perkin Elmer Lambda 35 spectrometer in particular with an RSAPE-20 reflectance spectroscopy accessory (Labsphere Inc., NorthSutton, NH, USA). The reflectance data were processed with the Kubelka-Munk $[F(R_\infty)]$ function through which the band gap was calculated graphing $[F(R_\infty) \times h\nu]^2$ vs. $h\nu$ (eV). Scanning electron microscopy (SEM) (Oxford instrument, UK) was used to characterize the morphology of the samples.

3.4. Photocatalytic Experiments

The reactor configuration used during the photocatalytic experiment was a cylindrical pyrex batch reactor (ID = 2.5 cm; height = 18 cm) equipped with an air distributor device

(flow rate of 170 cm³/min) filled with 100 mL of glyphosate (20 mg/L) aqueous solution. Generally, during the tests, 1.5 g/L of catalyst dosage was used. During the experiments, the glyphosate solution was continuously mixed by a peristaltic pump. Four visible lamps (PHILIPS nominal power: 8 W) with wavelength emission in the range 400–600 nm or solar simulated lamps (SUN-GLO 8W T5) with wavelength emission in the range 300–700 nm [33], or UV lamps (PHILIPS nominal power: 8 W) emitting in the range 200–400 nm were used as light sources. The lamps surrounded the photoreactor's external surface, positioned at a distance of about 30 mm from it; by doing so, the volume of the solution was irradiating uniformly [65]. The solution was left in dark condition for 1 h before switching on the light. The photocatalytic reaction was carried out under light irradiation up to 3 h. A given amount of solution was taken at a different time to evaluate the degradation and simultaneously mineralization of the pollutant present in the solution along the time. Moreover, additional control tests were carried out in the presence of glyphosate and irradiating the photoreactor with UV, solar or visible light (photolysis reaction) and in the absence of photocatalyst.

The degradation percentage (η) of glyphosate was calculated through Equation (5)

$$\eta = \left(1 - \frac{C}{C_0}\right) \times 100, \quad (5)$$

where C is the concentration (mg/L) during the irradiation time and C_0 is the initial concentration of the contaminant (mg/L);

The glyphosate mineralization was evaluated in terms of Total Organic Carbon (TOC) removal through Equation (6):

$$\text{TOC (removal \%)} = \left(1 - \frac{\text{TOC}_t}{\text{TOC}_0}\right) \times 100, \quad (6)$$

where TOC_0 is the initial TOC ($t = 0$) and TOC_t is the TOC value after a given irradiation time t . The TOC_0 of the reference aqueous solution is calculated from the initial glyphosate concentration used in the photocatalytic tests. The continuous mixing of the solution in the reactor was realized by bubbling compressed air ($Q = 170$ mL/min (STP–Standard Temperature and Pressure)), which also acts as a carrier for the gaseous species formed during the irradiation period. TOC of solution has been measured from CO_2 obtained by catalytic combustion at $T = 680$ °C. The reaction products in the gas phase were monitored by continuous gas analyzers (Uras 14, ABB) measuring the gaseous concentration of CO_2 at the outlet of the reactor. Subsequently, identified the best catalyst, photocatalytic tests for glyphosate degradation under different light irradiation were carried out. The effect of different catalyst dosage (0.375, 1.5, 3 g/L) and pH were also evaluated. Finally, in order to study the mechanism of deterioration, benzoquinone (1 mM), *i*-PrOH (10 mM), EDTA (0.2 mM) as radical scavengers were added to glyphosate aqueous solutions (10 mg/L). Subsequently, the degradation efficiency of glyphosate was detected under solar simulated lamps compared with glyphosate solution without scavenger.

3.5. Analytical Method for Glyphosate Quantification

The method used to detect glyphosate was proposed by Nagaraja, Besagarahally, and Bhaskara (2006) [66] and was optimized to find the best-operating conditions starting from 20 ppm of glyphosate solutions. It is characterized by a reaction of glyphosate with ninhydrin in presence of sodium molybdate, which forms a product of purple color with a maximum absorption at 570 nm [66]. A particular color “Ruhemann’s purple” product was formed when glyphosate reacts with ninhydrin in the presence of sodium molybdate in an aqueous neutral medium at 100°. In order to obtain a stable Ruhemann’s purple product with maximum absorption at 570 nm, 0.5% (*w/v*) of ninhydrin in the range 1.0–2.0 mL and 0.5% (*w/v*) of sodium molybdate in the range 1.0–3.0 mL were necessary. Hence, 0.5 mL of ninhydrin aqueous solution and 0.5 mL of sodium molybdate aqueous solution were selected to react with 2.5 mL of glyphosate solutions. The solution was kept in an oven at a temperature of 85 to 95 °C until the complete evaporation of the solution obtained a purple

color. Figure 11 is a representative behavior of glyphosate absorbance for its quantification, in which it is possible to see the maximum value of absorbance at 570 nm.

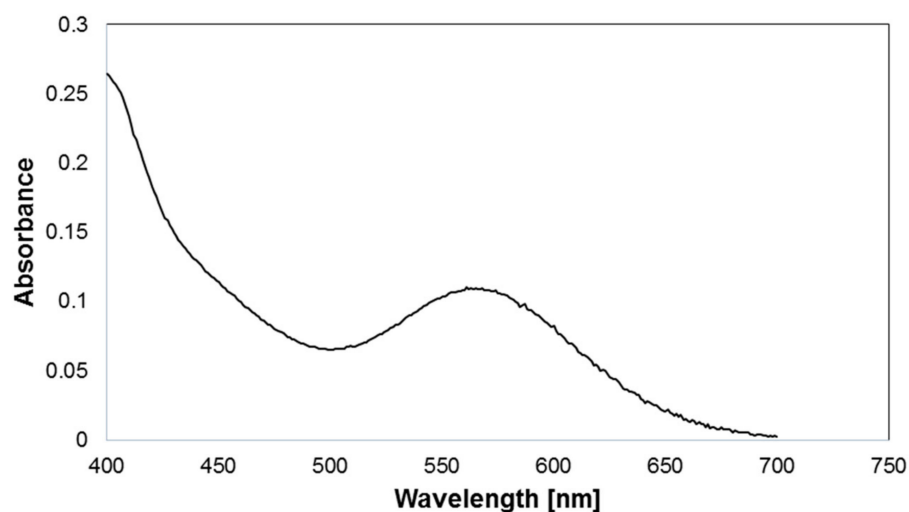


Figure 11. Representative behavior of glyphosate absorbance.

4. Conclusions

The results of this study clearly demonstrate that ZnO doped with tungsten can be used for the efficient degradation and mineralization of glyphosate under solar simulated lamps by the photocatalytic process. The improved photocatalytic behavior of this sample is due to several factors: the presence of W in its metallic oxidation state avoids the electron-hole recombination and the doping with W determined a reduction of bandgap energy ranging from 3.23 eV, typical of pure ZnO, to 3.19 eV. The characterization results confirmed the hexagonal wurtzite structure for all the prepared catalysts and average crystallite size in the range 38–40 nm. In particular, according to the results achieved in this work, 100 W-ZnO represents an interesting material to be used in photocatalytic glyphosate degradation with values of degradation and mineralization equal to 74% and 30% using solar simulated lamps in 180 min of irradiation, respectively. The possible irradiation with direct sunlight makes the process even more interesting because is an environmentally friendly process with zero energy costs. Studying the influence of the operating conditions, it was possible to observe that the highest glyphosate degradation was obtained with a photocatalyst dosage equal to 1.5 g/L, under neutral pH conditions. Finally, the photocatalytic performances of 100 W-ZnO were carried out analyzing the main reactive species involved during glyphosate degradation. Moreover, $O_2^{\bullet-}$ was shown to be the dominant reactive species in the photodegradation through a trapping experiment. This indicates that W-ZnO photocatalyst could be a promising candidate for the treatment of industrial wastewater containing glyphosate.

Supplementary Materials: The following are available online at <https://www.mdpi.com/2073-4344/11/2/234/s1>, Figure S1: Full isotherm for ZnO and 100W-ZnO samples, Figure S2: Influence of glyphosate initial concentration on degradation (a) and mineralization (b) after 180 min of solar simulated irradiation time.

Author Contributions: Conceptualization G.I. and M.R.; formal analysis, M.R.; investigation, G.I. and M.R.; data curation, V.V.; writing—original draft preparation, M.R.; writing—review and editing, G.I.; visualization, V.V. All authors have read and agreed to the published version of the manuscript.

Funding: This research received no external funding.

Institutional Review Board Statement: Not applicable.

Informed Consent Statement: Not applicable.

Data Availability Statement: Not applicable.

Conflicts of Interest: The authors declare no conflict of interest.

References

1. Sivagami, K.; Krishna, R.R.; Swaminathan, T. Photo catalytic degradation of pesticides in immobilized bead photo reactor under solar irradiation. *Sol. Energy* **2014**, *103*, 488–493. [[CrossRef](#)]
2. Costa, R.O.; Barcellos, P.S.; Canela, M.C.C. Removal of pesticide residues after conventional drinking water treatment: By-products and acetylcholinesterase inhibition. *Eclét. Quím. J.* **2018**, *48*, 65–73. [[CrossRef](#)]
3. Vagi, M.; Petsas, A. Advanced oxidation processes for the removal of pesticides from wastewater: Recent review and trends. In Proceedings of the 15th International Conference on Environmental Science and Technology, CEST2017, Rhodes, Greece, 31 August–2 September 2017.
4. Zobiole, L.H.S.; Kremer, R.; Oliveira, R.; Constantin, J. Glyphosate affects micro-organisms in rhizospheres of glyphosate-resistant soybeans. *J. Appl. Microbiol.* **2010**, *110*, 118–127. [[CrossRef](#)] [[PubMed](#)]
5. Sandrini, J.Z.; Rola, R.C.; Lopes, F.M.; Buffon, H.F.; Freitas, M.M.; Martins, C.d.M.G.; Da Rosa, C.E. Effects of glyphosate on cho-linesterase activity of the mussel *Perna perna* and the fish *Danio rerio* and *Jenynsia multidentata*: In vitro studies. *Aquat. Toxicol.* **2013**, *130*, 171–173. [[CrossRef](#)] [[PubMed](#)]
6. Chen, S.; Liu, Y. Study on the photocatalytic degradation of glyphosate by TiO₂ photocatalyst. *Chemosphere* **2007**, *67*, 1010–1017. [[CrossRef](#)]
7. Marin, P.; Bergamasco, R.; Módenes, A.N.; Paraiso, P.R.; Hamoudi, S. Synthesis and characterization of graphene oxide functionalized with MnFe₂O₄ and supported on activated carbon for glyphosate adsorption in fixed bed column. *Process Saf. Environ. Prot.* **2019**, *123*, 59–71. [[CrossRef](#)]
8. Tran, N.; Drogui, P.; Doan, T.L.; Le, T.S.; Nguyen, H.C. Electrochemical degradation and mineralization of glyphosate herbicide. *Environ. Technol.* **2017**, *38*, 2939–2948. [[CrossRef](#)]
9. Villamar-Ayala, C.A.; Carrera-Cevallos, J.V.; Vasquez-Medrano, R.; Espinoza-Montero, P.J. Fate, eco-toxicological characteristics, and treatment processes applied to water polluted with glyphosate: A critical review. *Crit. Rev. Environ. Sci. Technol.* **2019**, *49*, 1476–1514. [[CrossRef](#)]
10. Iervolino, G.; Vaiano, V.; Sannino, D.; Rizzo, L.; Sarno, G.; Ciambelli, P.; Isupova, L. Influence of operating conditions in the photo-Fenton removal of tartrazine on structured catalysts. *Chem. Eng. Trans.* **2015**, *43*, 979–984.
11. Iervolino, G.; Zammit, I.; Vaiano, V.; Rizzo, L. Limitations and Prospects for Wastewater Treatment by UV and Visible-Light-Active Heterogeneous Photocatalysis: A Critical Review. *Top. Curr. Chem.* **2020**, *378*, 7. [[CrossRef](#)] [[PubMed](#)]
12. Malakootian, M.; Shahesmaeili, A.; Faraji, M.; Amiri, H.; Martínez, S.S. Advanced oxidation processes for the removal of organophosphorus pesticides in aqueous matrices: A systematic review and meta-analysis. *Process Saf. Environ. Prot.* **2020**, *134*, 292–307. [[CrossRef](#)]
13. Zuorro, A.; Lavecchia, R.; Monaco, M.M.; Iervolino, G.; Vaiano, V. Photocatalytic Degradation of Azo Dye Reactive Violet 5 on Fe-Doped Titania Catalysts under Visible Light Irradiation. *Catalysts* **2019**, *9*, 645. [[CrossRef](#)]
14. Feng, C.; Deng, Y.; Tang, L.; Zeng, G.; Wang, J.; Yu, J.; Liu, Y.; Peng, B.; Feng, H.; Wang, J. Core-shell Ag₂CrO₄/N-GQDs@g-C₃N₄ composites with anti-photocorrosion performance for enhanced full-spectrum-light photocatalytic activities. *Appl. Catal. B Environ.* **2018**, *239*, 525–536. [[CrossRef](#)]
15. Feng, C.; Tang, L.; Deng, Y.; Wang, J.; Liu, Y.; Ouyang, X.; Chen, Z.; Yang, H.; Yu, J.; Wang, J. Maintaining stable LSPR performance of W₁₈O₄₉ by protecting its oxygen vacancy: A novel strategy for achieving durable sunlight driven photocatalysis. *Appl. Catal. B Environ.* **2020**, *276*, 119167. [[CrossRef](#)]
16. Feng, C.; Tang, L.; Deng, Y.; Wang, J.; Tang, W.; Liu, Y.; Chen, Z.; Yu, J.; Wang, J.; Liang, Q. Synthesis of branched WO₃@W₁₈O₄₉ homojunction with enhanced interfacial charge separation and full-spectrum photocatalytic performance. *Chem. Eng. J.* **2020**, *389*, 124474. [[CrossRef](#)]
17. Tang, L.; Feng, C.; Deng, Y.; Zeng, G.; Wang, J.; Liu, Y.; Feng, H.; Wang, J. Enhanced photocatalytic activity of ternary Ag/g-C₃N₄/NaTaO₃ photocatalysts under wide spectrum light radiation: The high potential band protection mechanism. *Appl. Catal. B Environ.* **2018**, *230*, 102–114. [[CrossRef](#)]
18. Chen, J.Q.; Hu, Z.J.; Wang, N.X. Photocatalytic mineralization of glyphosate in a small-scale plug flow simulation reactor by UV/TiO₂. *J. Environ. Sci. Health Part B* **2012**, *47*, 579–588. [[CrossRef](#)]
19. Chen, Y.; Wu, F.; Lin, Y.; Deng, N.; Bazhin, N.; Glebov, E. Photodegradation of glyphosate in the ferrioxalate system. *J. Hazard. Mater.* **2007**, *148*, 360–365. [[CrossRef](#)]
20. Echavia, G.R.M.; Matzusawa, F.; Negishi, N. Photocatalytic degradation of organophosphate and phosphonoglycine pesticides using TiO₂ immobilized on silica gel. *Chemosphere* **2009**, *76*, 595–600. [[CrossRef](#)] [[PubMed](#)]
21. Hosseini, N.; Toosi, M.R. Combined adsorption process and photocatalytic degradation of some commercial herbicides over N-doped TiO₂ particles supported on recyclable magnetic hexagonal mesoporous silica. *Sep. Sci. Technol.* **2018**, *54*, 1697–1709. [[CrossRef](#)]
22. Muneer, M.; Boxall, C. Photocatalyzed Degradation of a Pesticide Derivative Glyphosate in Aqueous Suspensions of Titanium Dioxide. *Int. J. Photoenergy* **2008**, *2008*, 1–7. [[CrossRef](#)]

23. Umar, K.; Aris, A.; Ahmad, H.; Parveen, T.; Jaafar, J.; Majid, Z.A.; Reddy, A.V.B.; Talib, J. Synthesis of visible light active doped TiO₂ for the degradation of organic pollutants—Methylene blue and glyphosate. *J. Anal. Sci. Technol.* **2016**, *7*, 725. [[CrossRef](#)]
24. Xue, W.; Zhang, G.; Xu, X.; Yang, X.; Liu, C.; Xu, Y. Preparation of titania nanotubes doped with cerium and their photocatalytic activity for glyphosate. *Chem. Eng. J.* **2011**, *167*, 397–402. [[CrossRef](#)]
25. Yang, Y.; Deng, Q.; Zhang, Y. Comparative study of low-index {1 0 1}-TiO₂, {0 0 1}-TiO₂, {1 0 0}-TiO₂ and high-index {2 0 1}-TiO₂ on glyphosate adsorption and photo-degradation. *Chem. Eng. J.* **2019**, *360*, 1247–1254. [[CrossRef](#)]
26. Iervolino, G.; Vaiano, V.; Rizzo, L.; Sarno, G.; Farina, A.; Sannino, D. Removal of arsenic from drinking water by photo-catalytic oxidation on MoOx/TiO₂ and adsorption on γ -Al₂O₃. *J. Chem. Technol. Biotechnol.* **2014**, *91*, 88–95. [[CrossRef](#)]
27. Khassin, A.A.; Yurieva, T.M.; Kaichev, V.V.; Bukhtiyarov, V.I.; Budneva, A.A.; Paukshtis, E.A.; Parmon, V.N. Metal–support interactions in cobalt-aluminum co-precipitated catalysts: XPS and CO adsorption studies. *J. Mol. Catal. A Chem.* **2001**, *175*, 189–204. [[CrossRef](#)]
28. Lee, J.C.; Park, S.; Park, H.-J.; Lee, J.-H.; Kim, H.-S.; Chung, Y.-J. Photocatalytic degradation of TOC from aqueous phenol solution using solution combusted ZnO nanopowders. *J. Electroceramics* **2009**, *22*, 110–113. [[CrossRef](#)]
29. Muruganandham, M.; Wu, J.J. Synthesis, characterization and catalytic activity of easily recyclable zinc oxide nanobundles. *Appl. Catal. B Environ.* **2008**, *80*, 32–41. [[CrossRef](#)]
30. Zammit, I.; Vaiano, V.; Iervolino, G.; Rizzo, L. Inactivation of an urban wastewater indigenous: Escherichia coli strain by cerium doped zinc oxide photocatalysis. *RSC Adv.* **2018**, *8*, 26124–26132. [[CrossRef](#)]
31. Vitiello, G.; Iervolino, G.; Imparato, C.; Rea, I.; Borbone, F.; De Stefano, L.; Aronne, A.; Vaiano, V. F-doped ZnO nano- and meso-crystals with enhanced photocatalytic activity in diclofenac degradation. *Sci. Total Environ.* **2021**, *762*, 143066. [[CrossRef](#)]
32. Vaiano, V.; Iervolino, G. Facile method to immobilize ZnO particles on glass spheres for the photocatalytic treatment of tannery wastewater. *J. Colloid Interface Sci.* **2018**, *518*, 192–199. [[CrossRef](#)]
33. Vaiano, V.; Iervolino, G.; Rizzo, L. Cu-doped ZnO as efficient photocatalyst for the oxidation of arsenite to arsenate under visible light. *Appl. Catal. B Environ.* **2018**, *238*, 471–479. [[CrossRef](#)]
34. Vaiano, V.; Chianese, L.; Rizzo, L.; Iervolino, G. Visible light driven oxidation of arsenite to arsenate in aqueous solution using Cu-doped ZnO supported on polystyrene pellets. *Catal. Today* **2021**, *361*, 69–76. [[CrossRef](#)]
35. Bora, L.V.; Mewada, R.K. Visible/solar light active photocatalysts for organic effluent treatment: Fundamentals, mechanisms and parametric review. *Renew. Sustain. Energy Rev.* **2017**, *76*, 1393–1421. [[CrossRef](#)]
36. Sun, J.-H.; Dong, S.-Y.; Feng, J.-L.; Yin, X.-J.; Zhao, X.-C. Enhanced sunlight photocatalytic performance of Sn-doped ZnO for Methylene Blue degradation. *J. Mol. Catal. A Chem.* **2011**, *335*, 145–150. [[CrossRef](#)]
37. Pelaez, M.; Nolan, N.T.; Pillai, S.C.; Seery, M.K.; Falaras, P.; Kontos, A.G.; Dunlop, P.S.; Hamilton, J.W.; Byrne, J.; O’Shea, K.; et al. A review on the visible light active titanium dioxide photocatalysts for environmental applications. *Appl. Catal. B Environ.* **2012**, *125*, 331–349. [[CrossRef](#)]
38. Cao, L.; Ma, D.; Zhou, Z.; Xu, C.; Cao, C.; Zhao, P.; Huang, Q. Efficient photocatalytic degradation of herbicide glyphosate in water by magnetically separable and recyclable BiOBr/Fe₃O₄ nanocomposites under visible light irradiation. *Chem. Eng. J.* **2019**, *368*, 212–222. [[CrossRef](#)]
39. Bechambi, O.; Sayadi, S.; Najjar, W. Photocatalytic degradation of bisphenol A in the presence of C-doped ZnO: Effect of operational parameters and photodegradation mechanism. *J. Ind. Eng. Chem.* **2015**, *32*, 201–210. [[CrossRef](#)]
40. Hanh, N.T.; Tri, N.L.M.; Van Thuan, D.; Tung, M.H.T.; Pham, T.-D.; Minh, T.D.; Trang, H.T.; Binh, M.T.; Nguyen, M.V. Monocrotophos pesticide effectively removed by novel visible light driven Cu doped ZnO photocatalyst. *J. Photochem. Photobiol. A Chem.* **2019**, *382*, 111923. [[CrossRef](#)]
41. Zong, Y.; Li, Z.; Wang, X.; Ma, J.; Men, Y. Synthesis and high photocatalytic activity of Eu-doped ZnO nanoparticles. *Ceram. Int.* **2014**, *40*, 10375–10382. [[CrossRef](#)]
42. Chen, D.; Gao, L.; Yasumori, A.; Kuroda, K.; Sugahara, Y. Size- and Shape-Controlled Conversion of Tungstate-Based Inorganic–Organic Hybrid Belts to WO₃ Nanoplates with High Specific Surface Areas. *Small* **2008**, *4*, 1813–1822. [[CrossRef](#)] [[PubMed](#)]
43. Chen, D.; Ye, J. Hierarchical WO₃ Hollow Shells: Dendrite, Sphere, Dumbbell, and Their Photocatalytic Properties. *Adv. Funct. Mater.* **2008**, *18*, 1922–1928. [[CrossRef](#)]
44. Wang, W.; Tadé, M.O.; Shao, Z. Research progress of perovskite materials in photocatalysis- and photovoltaics-related energy conversion and environmental treatment. *Chem. Soc. Rev.* **2015**, *44*, 5371–5408. [[CrossRef](#)] [[PubMed](#)]
45. Chang, X.; Sun, S.; Xu, X.; Li, Z. Synthesis of transition metal-doped tungsten oxide nanostructures and their optical properties. *Mater. Lett.* **2011**, *65*, 1710–1712. [[CrossRef](#)]
46. Li, D.; Haneda, H.; Ohashi, N.; Hishita, S.; Yoshikawa, Y. Synthesis of nanosized nitrogen-containing MOx–ZnO (M= W, V, Fe) composite powders by spray pyrolysis and their visible-light-driven photocatalysis in gas-phase acetaldehyde decomposition. *Catal. Today* **2004**, *93*, 895–901. [[CrossRef](#)]
47. Moafi, H.F.; Zanjanchi, M.A.; Fallah, S.A. Tungsten-doped ZnO nanocomposite: Synthesis, characterization, and highly active photocatalyst toward dye photodegradation. *Mater. Chem. Phys.* **2013**, *139*, 856–864. [[CrossRef](#)]
48. Subash, B.; Krishnakumar, B.; Swaminathan, M.; Shanthi, M. Enhanced photocatalytic performance of WO₃ loaded Ag–ZnO for Acid Black 1 degradation by UV–A light. *J. Mol. Catal. A Chem.* **2013**, *366*, 54–63. [[CrossRef](#)]
49. Shuo-wei, Z. Study on the Photocatalytic Degradation of Failure Glyphosate Pesticide by ZnO Nanoparticle. *J. Agro-Environ. Sci.* **2012**, *1*.

50. Faisal, M.; Ismail, A.A.; Ibrahim, A.A.; Bouzid, H.; Al-Sayari, S.A. Highly efficient photocatalyst based on Ce doped ZnO nanorods: Controllable synthesis and enhanced photocatalytic activity. *Chem. Eng. J.* **2013**, *229*, 225–233. [[CrossRef](#)]
51. Reddy, A.J.; Kokila, M.; Nagabhushana, H.; Rao, J.; Shivakumara, C.; Nagabhushana, B.; Chakradhar, R. Combustion synthesis, characterization and Raman studies of ZnO nanopowders. *Spectrochim. Acta Part A Mol. Biomol. Spectrosc.* **2011**, *81*, 53–58. [[CrossRef](#)] [[PubMed](#)]
52. Farid, S.; Mukherjee, S.; Sarkar, K.; Stroschio, M.A.; Dutta, M. Indium Dopant Concentration Effects on Zinc Oxide Nanowires. *J. Phys. Chem. A* **2019**, *123*, 8690–8695. [[CrossRef](#)]
53. Horzum, S.; Iyikanat, F.; Senger, R.T.; Çelebi, C.; Sbeta, M.; Yildiz, A.; Serin, T. Monitoring the characteristic properties of Ga-doped ZnO by Raman spectroscopy and atomic scale calculations. *J. Mol. Struct.* **2019**, *1180*, 505–511. [[CrossRef](#)]
54. Awan, S.U.; Hasanain, S.K.; Awan, M.S.; Shah, S.A. Raman scattering and interstitial Li defects induced polarization in co-doped multiferroic Zn_{0.96-y}Co_{0.04}Li_yO (0.00 ≤ y ≤ 0.10) nanoparticles. *RSC Adv.* **2015**, *5*, 39828–39839. [[CrossRef](#)]
55. Pal, U.; Kim, C.W.; Jadhav, N.A.; Kang, Y.S. Ultrasound-Assisted Synthesis of Mesoporous ZnO Nanostructures of Different Porosities. *J. Phys. Chem. C* **2009**, *113*, 14676–14680. [[CrossRef](#)]
56. Ba-Abbad, M.M.; Kadhum, A.A.H.; Mohamad, A.B.; Takriff, M.S.; Sopian, K. Visible light photocatalytic activity of Fe³⁺-doped ZnO nanoparticle prepared via sol-gel technique. *Chemosphere* **2013**, *91*, 1604–1611. [[CrossRef](#)] [[PubMed](#)]
57. Zhang, L.; Yang, Y.; Fan, R.; Yu, J.; Li, L. Improving the efficiency of ZnO-based dye-sensitized solar cells by Pr and N co-doping. *J. Mater. Chem. A* **2003**, *1*, 12066–12073. [[CrossRef](#)]
58. Ngom, B.; Mpahane, T.; Manyala, N.; Nemraoui, O.; Buttner, U.; Kana, J.; Fasasi, A.; Maaza, M.; Beye, A. Structural and optical properties of nano-structured tungsten-doped ZnO thin films grown by pulsed laser deposition. *Appl. Surf. Sci.* **2009**, *255*, 4153–4158. [[CrossRef](#)]
59. Assalin, M.R.; De Moraes, S.G.; Queiroz, S.C.N.; Ferracini, V.L.; Duran, N. Studies on degradation of glyphosate by several oxidative chemical processes: Ozonation, photolysis and heterogeneous photocatalysis. *J. Environ. Sci. Heal. Part B* **2009**, *45*, 89–94. [[CrossRef](#)]
60. Xu, X.; Ji, F.; Fan, Z.; He, L. Degradation of glyphosate in soil photocatalyzed by Fe₃O₄/SiO₂/TiO₂ under solar light. *Int. J. Environ. Res. Public Health* **2011**, *8*, 1258–1270. [[CrossRef](#)] [[PubMed](#)]
61. Anandan, S.; Vinu, A.; Lovely, K.S.; Gokulakrishnan, N.; Srinivasu, P.; Mori, T.; Murugesan, V.; Sivamurugan, V.; Ariga, K. Photocatalytic activity of La-doped ZnO for the degradation of monocrotophos in aqueous suspension. *J. Mol. Catal. A Chem.* **2007**, *266*, 149–157. [[CrossRef](#)]
62. Daskalaki, V.M.; Kondarides, D.I. Efficient production of hydrogen by photo-induced reforming of glycerol at ambient conditions. *Catal. Today* **2009**, *144*, 75–80. [[CrossRef](#)]
63. Daneshvar, N.; Salari, D.; Khataee, A. Photocatalytic degradation of azo dye acid red 14 in water on ZnO as an alternative catalyst to TiO₂. *J. Photochem. Photobiol. A Chem.* **2004**, *162*, 317–322. [[CrossRef](#)]
64. Comparelli, R.; Fanizza, E.; Curri, M.; Cozzoli, P.; Mascolo, G.; Agostiano, A. UV-induced photocatalytic degradation of azo dyes by organic-capped ZnO nanocrystals immobilized onto substrates. *Appl. Catal. B Environ.* **2005**, *60*, 1–11. [[CrossRef](#)]
65. Iervolino, G.; Vaiano, V.; Sannino, D.; Rizzo, L.; Palma, V. Enhanced photocatalytic hydrogen production from glucose aqueous matrices on Ru-doped LaFeO₃. *Appl. Catal. B Environ.* **2017**, *207*, 182–194. [[CrossRef](#)]
66. Bhaskara, B.L.; Nagaraja, P. Direct sensitive spectrophotometric determination of glyphosate by using ninhydrin as a chromogenic reagent in formulations and environmental water samples. *Helv. Chim. Acta* **2006**, *89*, 2686–2693. [[CrossRef](#)]